REPORT DOCUMENTATION PAGE

Form Approved OMB NO. 0704-0188

1. REPORT DATE (DD-MM-YYYY)	2. REPORT TYPE	3. DATES COVERED (From - To)
	New Reprint	-

4. TITLE AND SUBTITLE
MOF-Graphite Oxide Nancomposites: Surface Characterization and Evaluation as Adsorbents of Ammonia

5a. CONTRACT NUMBER
W911NF-05-1-0537

5b. GRANT NUMBER

5c. PROGRAM ELEMENT NUMBER
306033

6. AUTHORS
C.Petit, T.J. Bandosz

5d. PROJECT NUMBER

5e. TASK NUMBER

5f. WORK UNIT NUMBER

7. PERFORMING ORGANIZATION NAMES AND ADDRESSES
CUNY - City College of New York (Flushing)
65-30 Kissena Blvd.
Flushing, NY 11367 -

8. PERFORMING ORGANIZATION REPORT NUMBER

9. SPONSORING/MONITORING AGENCY NAME(S) AND ADDRESS(ES)
U.S. Army Research Office
P.O. Box 12211
Research Triangle Park, NC 27709-2211

10. SPONSOR/MONITOR'S ACRONYM(S)
ARO

11. SPONSOR/MONITOR'S REPORT NUMBER(S)
49397-CH.31

12. DISTRIBUTION AVAILIBILITY STATEMENT
Approved for public release; federal purpose rights

13. SUPPLEMENTARY NOTES
The views, opinions and/or findings contained in this report are those of the author(s) and should not contrued as an official Department of the Army position, policy or decision, unless so designated by other documentation.

14. ABSTRACT
see the attached

15. SUBJECT TERMS
adsorption on ammonia

16. SECURITY CLASSIFICATION OF:			17. LIMITATION OF ABSTRACT	15. NUMBER OF PAGES	19a. NAME OF RESPONSIBLE PERSON
a. REPORT	b. ABSTRACT	c. THIS PAGE			Teresa Bandosz
UU	UU	UU	UU		19b. TELEPHONE NUMBER: 212-650-6017

Report Title

MOF-Graphite Oxide Nancomposites: Surface Characterization and Evaluation as Adsorbents of Ammonia

ABSTRACT

see the attached

REPORT DOCUMENTATION PAGE (SF298)
(Continuation Sheet)

Continuation for Block 13

ARO Report Number 49397.31-CH
MOF-Graphite Oxide Nancomposites: Surface C ...

Block 13: Supplementary Note

Approved for public release; federal purpose rights

MOF–graphite oxide nanocomposites: surface characterization and evaluation as adsorbents of ammonia

Camille Petit and Teresa J. Bandosz*

Received 5th May 2009, Accepted 13th June 2009
First published as an Advance Article on the web 15th July 2009
DOI: 10.1039/b908862h

Metal-organic framework (MOF-5)–graphite oxide (GO) composite was synthesized using a solvothermal synthesis route. The parent materials (MOF-5 and GO) and the nanocomposite were characterized using X-ray diffraction, SEM, TEM, FTIR and adsorption of nitrogen. They were also tested as adsorbents of ammonia in dynamic conditions. The composite material obtained had a unique layered texture with a preserved structure of MOF-5 and GO. When tested as ammonia adsorbent, the composite showed some synergy enhancing the adsorption capacity in comparison with the hypothetical physical mixture of the components. Although the removal capacity was high in the presence of moisture, water had a detrimental effect on the chemistry of materials and destroyed their porous framework. This caused ammonia retained on the surface to be progressively desorbed from the materials when the samples were purged with air.

Introduction

Graphite oxide (GO), formed by treating graphite with very strong oxidizing agents such as $KClO_3/HNO_3$,[1] has a layered structure and a non-stochiometric chemical composition, which depends on the level of oxidation. Recent advances in the synthesis and experimental characterization[2–5] of GO provide the possibility of controlling the structure and surface chemistry of these materials, leading to renewed interest in them as adsorbents, and particularly as reactive adsorbents.[6,7] The graphene layers of GO are arranged in an organized way with the interlayer distance varying from 6 to 12 Å. The main reason for these variations in interlayer distance is the level of hydration.[2] Since epoxy and hydroxyl groups exist within the interlayer space, the water molecules are attracted there *via* hydrogen bonding.[2] Moreover, both functional groups and water molecules have different types of motion depending on the location of water, which can be either embedded or distributed in interlayer voids.

The layered character of graphite oxide opened a new route for the synthesis of composite materials.[8–19] This path is possible owing to the hydrophilic character of GO, its easy dispersion in water and delamination in alkaline media or alcohols.[20,21] Moreover, graphite layers can be easily restacked and their degree of orientation depends on the method of drying. Our recent studies demonstrate that graphite oxide can be an efficient adsorbent of ammonia.[6,7,22] NH_3 reacts with the acidic groups located on the edges of graphene layers and is also intercalated between the graphene sheets where hydrogen bonding with epoxy groups is the predominant adsorption mechanism. The amount of ammonia adsorbed on GO is very high in comparison with activated carbons.[6,7,22,23]

Department of Chemistry, The City College and the Graduate School of the City University of New York, 160 Convent Avenue, New York, NY, 10031, USA. E-mail: tbandosz@ccny.cuny.edu; Fax: +1 212 650 6107; Tel: +1 212 650 6017

Another group of interesting materials are metal–organic frameworks (MOFs).[24–34] Their synthesis and properties were described in detail by Yaghi and co-workers.[24–27] They showed that intermolecular interactions and metal–ligand coordinations may be used to design a wide variety of 2-D and 3-D metal–organic networks with high porosity, unusual ion exchange and adsorptive properties.[35,36] Examples are MOF-*n* materials which are built from the extended analogues of molecular metal carboxylate clusters.[26] They are stable at rather high temperature and their porosity reaches 60%.[35] The preparation of MOFs involves reaction between solutions of metal species and organic linkers. The structure obtained is the result of maximum degrees of freedom of both components, spherical shape of metal ions and well-defined points of contacts for the organic linker. A detailed summary of the factors affecting the reticular chemistry of those materials is presented in ref. 29. Besides a broad range of transition metals, which are used in the synthesis, also noble metals can expand the catalytic features of these materials.[30]

Well-defined framework and high porosity with a broad range of pore sizes make MOFs potentially good adsorbents for air purification and separation.[36–41] So far adsorption of species such as hydrogen,[37–39] carbon dioxide[40] or methane[41] has been studied. Recently, Yaghi and co-workers studied the adsorption of various harmful gases using several types of MOF-*n* materials.[36] Improvement compared to a common activated carbon (BPL carbon) was observed, especially in the retention of ammonia.[36] An interesting summary of industrial applications of MOFs is presented in ref. 38 with examples of the superiority of this kind of materials toward adsorption of tetrahydrothiophene, amines, ammonia and alcohols. These materials also show a good performance in gas storage under high pressure.

Taking into account the above, a major goal of this research is to present the synthesis of MOF–GO nanocomposite materials, which combine the favorable attributes of carbonaceous surfaces and MOFs. In particular, GO should potentially lead to an enhancement in nonspecific adsorption owing to the presence of

extended graphene type layers and also to an enhancement in strong specific adsorption owing to its acidic character. On the other hand, MOF can improve the kinetics of adsorption due to the structure of its framework. Moreover, the specific interactions and reactivity can also be enhanced owing to MOF's chemical composition. MOF-5 was chosen in this study as the MOF-*n* compound. In this material, $[Zn_4O]^{6+}$ tetrahedra form the corners of the resulting primitive cubic structure, while benzene carboxylates (1,4-benzenedicarboxylate, BDC) allow the junction between these zinc oxide clusters.[42] The formula of the resulting material is $Zn_4O(H\text{-}BDC)_3$.[35] Synthesis of the parent materials and the nanocomposite is followed by their surface characterization using a range of experimental methods. Then, their performance in adsorption of ammonia is evaluated. To the best of our knowledge, we are the first group reporting the synthesis and characterization of such a material.

Experimental

Synthesis of materials

Graphite oxide was synthesized by oxidation of graphite (Sigma-Aldrich) using the Hummers method.[43] Briefly, graphite powder (10 g) was stirred with cold concentrated sulfuric acid (230 mL at 0 °C). Then, potassium permanganate (30 g) was added to the suspension slowly to prevent a rapid rise in temperature (less than 20 °C). The reaction mixture was then cooled to 2 °C. After removal of the ice-bath, the mixture was stirred at room temperature for 30 min. Distilled water (230 mL) was slowly added to the reaction vessel to keep the temperature under 98 °C. The diluted suspension was stirred for an additional 15 min and further diluted with distilled water (1.4 L), before adding hydrogen peroxide (100 mL). The mixture was left overnight. GO particles, settled at the bottom, were separated from the excess liquid by decantation followed by centrifugation. The remaining suspension was transferred to dialysis tubes (MW cutoff 6000–9000). Dialysis was carried out until no precipitate of $BaSO_4$ was detected by addition of $BaCl_2$. Then, the wet form of graphite oxide was centrifuged and freeze-dried. A fine brown powder of the initial graphite oxide was obtained. The resulting material is referred to as GO.

MOF-5 was prepared by mixing zinc nitrate hexahydrate (10.4 g) and 1,4-benzenedicarboxylate (2 g) in *N*,*N*-dimethylformamide (DMF, 140 mL) until complete dissolution of the solids. Then, the mixture was transferred into a round-bottom flask connected to a condenser and heated at 115–120 °C for 24 h. After cooling, the supernatant was removed and the crystals deposited on the bottom of the flask were collected, washed with DMF, and immersed in fresh chloroform overnight. Chloroform was changed twice over the course of two days. Finally, crystals were collected, placed inside a closed filtering flask connected to an aspirator used to create vacuum inside the flask, and heated at 130–135 °C for 6 h. The resulting crystals were then kept in a dessicator.

The composite material was prepared by dispersing GO powder in the well-dissolved zinc nitrate–BDC mixture. The resulting suspension was subsequently stirred and subjected to the same synthesis procedure as for MOF-5. The added GO consists of 5 wt% of final material. The synthesized composite is referred to as MOF-5–GO.

Methods

Ammonia adsorption

Adsorption capacity for the removal of ammonia was assessed by carrying out dynamic tests at room temperature. In this process, a flow of ammonia diluted in air went through a fixed bed of an adsorbent sample.[22,23] The total flow rate of the inlet gas was 450 mL min^{-1} with an ammonia concentration of 1000 ppm. The adsorbent bed contained about 1.5 cc of the adsorbent powder (GO, MOF-5 or MOF-5–GO) packed into a glass column. The size of the bed was 20 mm (height) × 10 mm (diameter). The conditions were chosen to accelerate the time of the test and limit the exposure of the sensor, the lifetime of which is relatively short. The ammonia concentration in the outlet gas was measured using a Multi-Gas Monitor ITX system. The adsorption capacity of each sample was then calculated in milligrams per gram of sorbent, as the difference between the inlet and outlet concentrations multiplied by the inlet flow rate, the breakthrough time and the ammonia molar mass in the experimental conditions. To evaluate the influence of water, the experiments for all carbon samples were performed with a flow of ammonia gas diluted either in dry air (ED) or in moist air (70% humidity) (EM). On all samples, the desorption of ammonia was evaluated when exposed to 360 mL min^{-1} of the carrier air.

Textural characterization

Textural characterization was carried out by measuring the N_2 adsorption isotherms at −196 °C. Before the experiments, the samples were outgassed under vacuum at 120 °C. The isotherms were used to calculate the specific surface area, S_{BET}, total pore volume, V_t, volume of micropores, V_{mic}, volume of mesopores, V_{mes}, and pore size distributions. The latter was calculated using the density functional theory (DFT).[44]

Surface pH

The pH of a sample suspension provides information about the acidity and basicity of the surface. About 0.15 g of the initial and exhausted MOF-5, GO or MOF-5–GO powder was added to 7.5 mL of distilled water. The suspension was stirred overnight to reach equilibrium before recording the pH.

SEM

Scanning electron microscopy was performed on a Zeiss Supra 55 instrument. The instrument has a resolution of 5 nm at 30 kV. Scanning was performed on a sample powder previously dried and sputter coated with a thin layer of carbon to avoid charging.

TEM

Transmission electron microscopy (TEM) was performed on a Zeiss EM 902 instrument. The microscope has a line resolution of 0.34 nm and a point resolution of 0.5 nm and operates in normal diffraction and low dose modes at 50 or 80 kV. Analyses were performed after the samples were resuspended in ethanol.

XRD

X-Ray diffraction (XRD) measurements were conducted using standard powder diffraction procedures. Adsorbents were ground with DMF in a small agate mortar. The mixture was smear-mounted onto a glass slide and then analyzed by Cu Kα radiation generated in a Philips X'Pert X-ray diffractometer. A standard glass slide was run for the background correction.

FTIR

Fourier transform infrared (FTIR) spectroscopy was carried out using a Nicolet Magna-IR 830 spectrometer using the attenuated total reflectance (ATR) method. The spectrum was generated and collected 16 times and corrected for the background noise. The experiments were done on the powdered samples, without KBr addition.

Results and discussion

Metal–organic frameworks or graphite oxides are expected to have a distinct structure, which provides fingerprints of their textural and chemical nature. To ensure that the MOF-5–GO composite has the elements of both components, the X-ray diffraction patterns should be analyzed. They are collected in Fig. 1. For GO, the well-defined peak at 2Θ about 9.29° represents an interlayer distance of 9.50 Å. For MOF-5, various sharp diffraction peaks are seen which are characteristic of this material structure and are in agreement with the data published in the literature.[45–47] The XRD pattern of the nanocomposite does not differ significantly from that for MOF-5. Only the sharpness of the peak at 2Θ about 9.7° is slightly reduced and the splitting of that peak is noticed. This split was observed by Lillerud and co-workers on MOF-5 and attributed to a distortion of the cubic symmetry.[46] Finding it for our composite suggests that the presence of GO in the sample increases the distortion in the MOF-5 cubic arrangement, as one could expect owing to additional constraints in the degrees of freedom during synthesis. Nevertheless, X-ray analyses indicate that the major structural and chemical features of MOF-5 are preserved in MOF-5–GO. The predominant features of MOF-5 are expected since it consists of 95 wt% of the nanocomposite content.

The texture of the materials studied is seen on SEM micrographs presented in Fig. 2. For MOF-5, besides the well-defined cubic crystals, some remains of an amorphous phase can be distinguished. The particles of GO look very dense with the layers stacked together as a result of dispersive forces and strong specific interactions between the surface groups on the graphene-like layers. On the other hand, MOF-5–GO exhibits totally different surface features. The layers of sandwich-like structures can be clearly seen and the regular structure of layers suggests that they might be layers of MOF-5 crystallites separated by the layers of GO. In spite of the fact that only 5 wt% GO were added during the MOF-5 synthesis, its effect on the texture of materials is very pronounced. It is interesting that in the synthesis crystallites of similar sizes are formed and then restacked into larger particles with GO layers acting as dividers. The differences in the texture between MOF-5–GO composite, MOF-5 and GO precursors are also visible in TEM micrographs (Fig. 3). On MOF-5–GO, ordered layered units with random orientation can

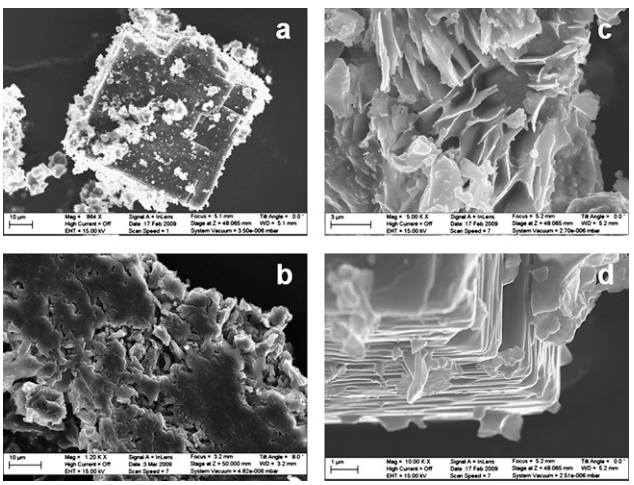

Fig. 2 SEM micrographs for the parent materials and the nanocomposite: (a) MOF-5, (b) GO, (c) and (d) MOF-5–GO.

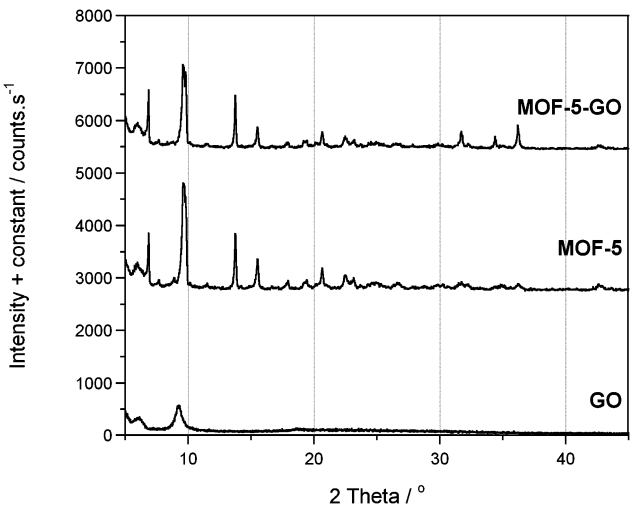

Fig. 1 X-Ray diffraction patterns for the parent materials and the nanocomposite.

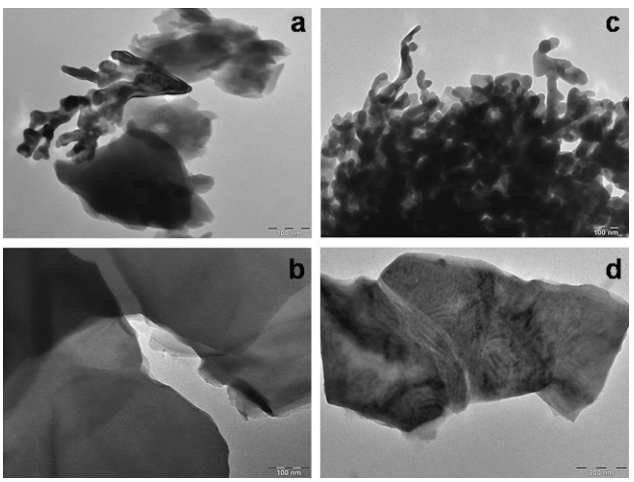

Fig. 3 TEM micrographs for the parent materials and the nanocomposite: (a) MOF-5, (b) GO, (c) and (d) MOF-5–GO.

be distinguished. We hypothesize, taking into account the chemistries of both components of nanocomposites, that the building process of the ordered structure of MOF-5–GO is based on the attachments of MOF-5 "blocks" to a graphene layer by reactions with epoxy groups on GO. This follows the analysis of water interactions with MOF-5 presented by Greathouse and Allendorf[48] where a replacement of an oxygen atom in ZnO_4 tetrahedron by an oxygen atom from water is a very important step leading to the decomposition of MOF-5 by water. In our view oxygen atoms in epoxy groups on GO play the same role as oxygen atoms in water.[49] In the subsequent steps of the nanocomposite building process, an alternation between attachment of graphene layers and MOF-5 "blocks" takes place.

The nitrogen adsorption isotherms measured on MOF-5 and MOF-5–GO exhibit a typical Langmuir-type shape suggesting the predominant microporosity (Fig. 4). The surface of GO is inaccessible for the nitrogen molecule and thus this material is considered as nonporous.[22] The parameters of the porous structure calculated from these isotherms and pore size distributions (PSDs) are presented in Table 1 and Fig. 5, respectively. Although the surface area of MOF-5 is smaller than 3000–3500 $m^2\ g^{-1}$, observed for some MOF-5,[26,45] surfaces of similar magnitude to our material were reported by Huang and co-workers, and Panella and Hirscher.[47,50] This low surface area can be related to the method of outgassing during the preparation and thus the completeness of solvent removal. The solvent

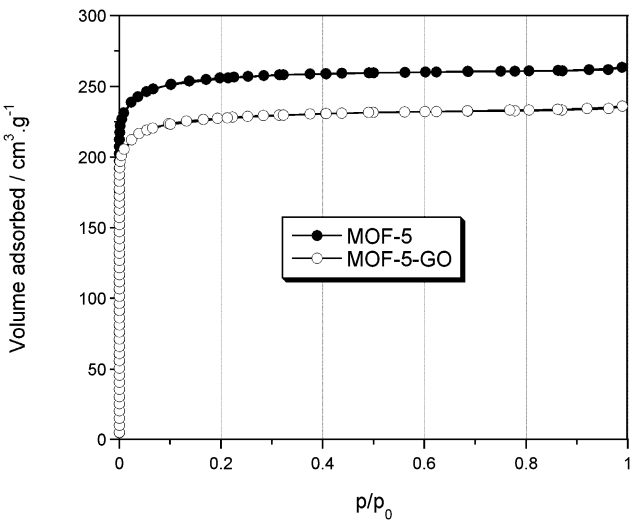

Fig. 4 Nitrogen adsorption isotherms for the initial samples.

Table 1 Parameters of porous structure calculated from nitrogen adsorption isotherms

Sample	S_{BET}/ $m^2\ g^{-1}$	V_t/ $cm^3\ g^{-1}$	V_{meso}/ $cm^3\ g^{-1}$	V_{mic}/ $cm^3\ g^{-1}$	V_{mic}/ V_t
MOF	793	0.408	0.023	0.385	0.94
MOF–ED	739	0.399	0.010	0.389	0.97
MOF–EM	10	0.057	0.052	0.005	0.09
MOF–GO	706	0.365	0.024	0.341	0.93
MOF–GO–ED	710	0.365	0.024	0.341	0.93
MOF–GO–EM	8	0.025	0.021	0.004	0.16

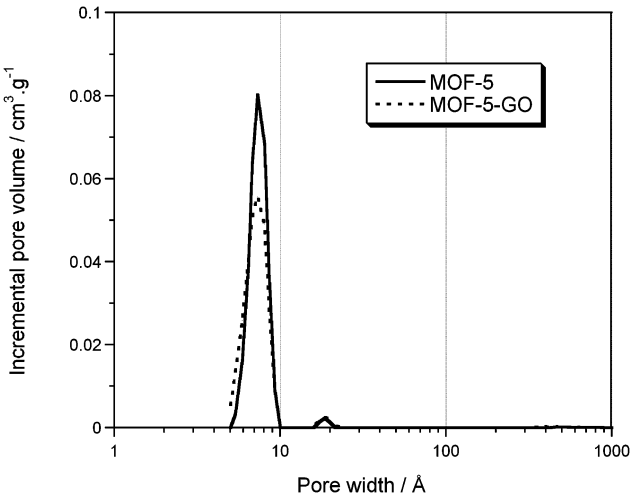

Fig. 5 Pore size distributions for the initial samples.

used to prepare the materials as well as the temperature at which crystals were formed might also have an influence on their resulting porosity.[38,45] The materials obtained are predominantly microporous with pore size between 5 and 10 Å (Fig. 5), which is in agreement with the structural model of cavities in MOF-5 in which the passage of spheres of diameter up to 8.0 Å has been defined.[42] Pores with sizes between 16.0 and 23.5 Å are also found for our materials and they might be due to a distortion in the structure of MOF-5. When the nanocomposite is formed, the structural parameters decrease by about 10%, and the pore size distribution is preserved. Results for PSDs must be considered with caution since the pore model used for DFT calculation reflects the slit-shaped pores of carbonaceous materials.[44] Nevertheless, since the same model is used for the series of materials the trends in PSDs can be analyzed.

The ammonia adsorption capacities calculated from the breakthrough curves (Fig. 6) in milligrams per gram of the materials and in milligrams per unit volume of the adsorbent bed and the surface pH values for the initial and exhausted samples

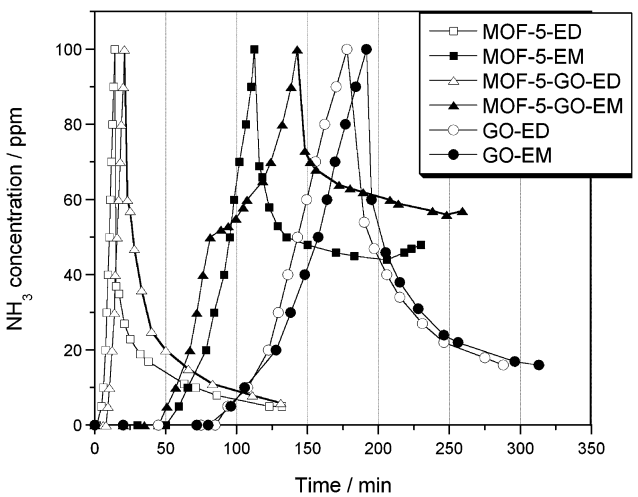

Fig. 6 Ammonia breakthrough curves and desorption curves for MOF-5, GO and MOF-5–GO.

Table 2 Measured ammonia breakthrough capacity, calculated hypothetical capacity and the surface pH for the initial and exhausted samples

Sample	NH_3 breakthrough capacity		Calculated hypothetical capacity	pH	
	mg g^{-1} of material	mg cm^{-3} of material	mg g^{-1} of material	Initial	Exhausted
GO-ED	55.5	36.9	—	2.47	6.24
GO-EM	61.0	39.8	—	2.47	6.66
MOF–ED	5.9	2.9	—	5.64	5.80
MOF–EM	42.5	23.0	—	5.64	6.63
MOF–GO–ED	6.9	3.3	8.4	6.09	6.10
MOF–GO–EM	53.3	28.8	43.4	6.09	7.06

are summarized in Table 2. In this table, we also list the capacities calculated by considering the physical mixture of the adsorbents (5 wt% GO and 95 wt% MOF-5). It has to be noted that the error in the NH_3 breakthrough capacities is around 10%. Even though the capacity in moist conditions on the MOF-5–GO is smaller than that on GO, the value obtained is about 12% greater than that expected when the structural synergy between the components of the nanocomposite does not exist. High adsorption on GO was explained by interactions of ammonia with acidic groups and its intercalation between the distorted graphitic layers.[6,22] In dry air, the performance of MOF-5 is very poor and the capacity measured is consistent with that reported by Yaghi *et al.*[36] That low capacity is a result of the lack of strong chemical interactions between NH_3 and MOF compound[36] and relatively large pores compared to the size of the ammonia molecule (3 Å[51]). The much higher capacity in wet conditions must be related to adsorption of large quantities of water on MOF-5[52] and dissolution of ammonia in the water present in the pore space. Another possible scenario is a change in the mechanism of adsorption caused by the formation of ammonium ions simultaneously with changes in the chemistry of materials caused by water[50] as will be discussed later in this paper. The low capacity of the composite at dry conditions is governed by the behavior of the predominant phase of MOF-5. The presence of GO in the composite slightly increases the performance but the analysis is difficult owing to a very short breakthrough time.

In spite of the lower NH_3 removal capacity in wet conditions on MOF-5 than that on GO, the performance is still better than that on unmodified activated carbons,[52–54] comparable to those on carbons modified with metal chlorides,[23] and slightly better than that measured on carbons modified with polyoxometalates[55,56] or metal oxides.[57–59] Since the capacity is high even though the pH is much higher than that for GO, other mechanisms than simple acid–base interactions must be involved in the retention of ammonia on those materials. It is interesting that on the exhausted samples (for MOF-5 and MOF-5–GO), the pH increases by only one pH unit after exposure to ammonia in spite of the high capacity. For this, a neutralization reaction or removal of a significant amount of ammonia dissolved in water by purging with dry air after the adsorption process is the possible explanation.

Analysis of the shapes of the NH_3 breakthrough curves and the desorption curves indicates the differences in the performance of materials. It has to be mentioned here that due to the sensor performance limitations, the desorption tests were performed only for 2 h after the adsorption tests and that this period might not be sufficient to observe the full desorption. The relatively small area under the desorption curve in the case of GO run in moist and dry conditions indicates a significant quantity of strongly adsorbed ammonia.[22] For MOF-5, initially a sharp decrease in the concentration is noticed on the desorption curve and then ammonia concentration in the air stream stays at a more or less constant level during the duration of the desorption experiment. A similar pattern is noticed for the nanocomposite. This must be related to the removal of water with dissolved ammonia. That process is expected to last a long time when very small size pores are present.[60] All these are signs of a weak retention of ammonia. Moreover, as the parameters of porous structure indicate, after ammonia adsorption in moist conditions, the materials (MOF-5 and MOF-5–GO) become practically nonporous (see Table 1). This loss of porosity is due to a collapsing of the structure, as a result of water exposure, as already observed by Long and co-workers.[45] As mentioned above, Greathouse and Allendorf showed that water leads to the destruction of the MOF-5 structure owing to its specific interactions with the zinc oxide clusters.[48] Oxygen atoms in water progressively replace oxygen atoms in ZnO_4 tetrahedra. Hydrogen bonding between hydrogen atoms in water and oxygen atoms in ZnO_4 tetrahedra represents another way of interactions leading to the collapse of the MOF-5 structure. That destruction might affect the kinetics of water desorption (with dissolved ammonia). It is also possible that the destruction happens gradually when ammonia is present in the system. Indeed, ammonia might compete with water for reaction sites owing to some similarities in the chemistries of these two species. In particular, hydrogen bonding between hydrogen atoms in NH_3 and oxygen atoms in ZnO_4 tetrahedron appears as a plausible scenario. Support for this might be that observed increase in the ammonia concentration at the end of the desorption experiment. It is interesting that the structure does not collapse when it is exposed only to ammonia.

Another interesting feature on the breakthrough curves of the composite tested in moist conditions is a well-pronounced change in the shape of the curve with the progress of adsorption starting at a concentration of 50 ppm. This behavior is real and is not seen for GO or MOF-5. This suggests changes in the mechanism of adsorption or appearance of additional adsorption centers with the duration of the experiment. The changes in the chemistry can be only caused by either water or ammonia, or ammonia and water.

How ammonia changes the chemistry of the composite is seen on the FTIR spectra presented in Fig. 7. The spectra for GO before and after adsorption of ammonia were analyzed in detail previously.[58,61,62] As expected based on the composition of the

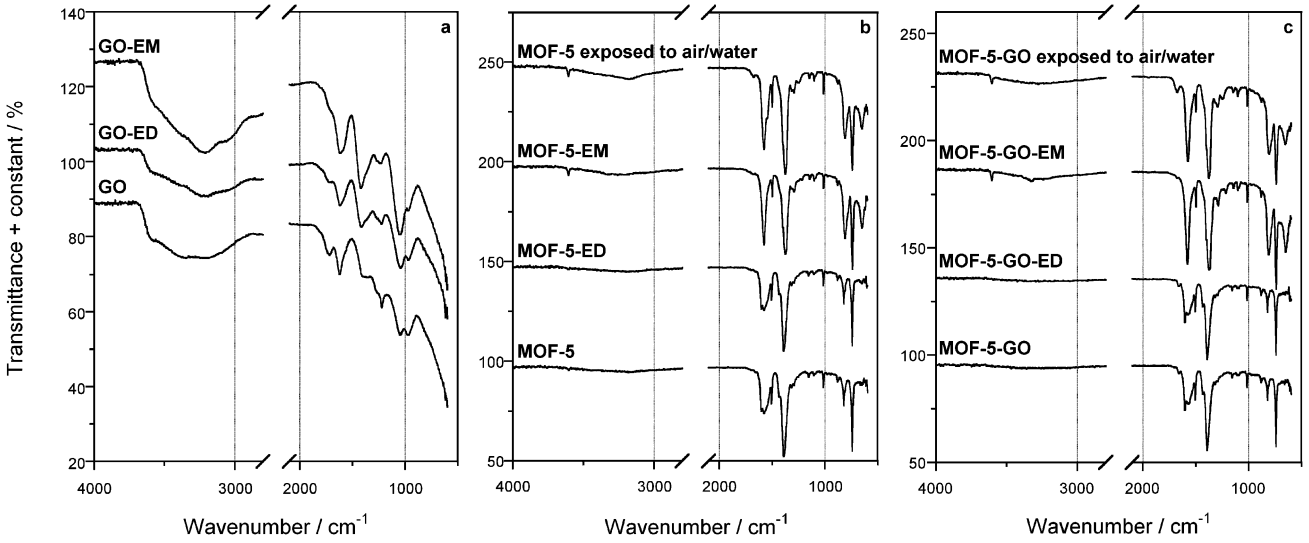

Fig. 7 FTIR spectra for the initial and exhausted samples: (a) GO, (b) MOF-5, (c) MOF-5–GO.

MOF-5–GO, the spectrum for the nanocomposite resembles that for MOF-5. The bands at 1510 $cm^{-1}$and 1580 cm^{-1} are attributed to the asymmetric stretching of carboxylic groups in BDC whereas the one at 1390 cm^{-1} is due to the symmetric stretching of carboxylic groups in BDC.[62,63] In the region 1300–700 cm^{-1}, several bands are observed and they are assigned to the out-of-plane vibrations of BDC.[63,64] After adsorption of ammonia in dry air, the spectra of both MOF-5 and MOF-5–GO do not change. However, in moist conditions, new bands at 660 cm^{-1}, 1230 cm^{-1}, 1300 cm^{-1}, 3200 and 3610 cm^{-1} appear for MOF-5 and MOF-5–GO. The latter changes observed in the range 600–1600 cm^{-1} must be due to the collapsing of the MOF-5 structure and change in the environment of the carboxylic groups and the zinc oxide. Indeed, taking into account the proposed mechanism of destruction of the MOF-5 framework by water,[48] carboxylic groups are "released" during this collapsing which must induce modifications in the vibrations at about 1600 cm^{-1}. A well-defined band at 3610 cm^{-1} indicates the presence of strongly bound water.[47] A broad band at ~3200 cm^{-1} must be due to the overlapping bands from O–H and N–H vibrations in water and ammonia, respectively.[65] Comparison of the spectra obtained for MOF-5–EM and MOF-5–GO–EM with the corresponding ones obtained after exposure to a flow of humid air shows as a main difference a band at 1685 cm^{-1} for samples run in humid air only. This band suggests the presence of protonated carboxylic groups in BDC.[66] The fact that it is not observed for MOF-5–EM and MOF-5–GO–EM even though water is present suggests that ammonia interacts with those carboxylic groups. Indeed, carboxylic groups formed in this process might anchor ammonia ions *via* acid–base reaction. This finding explains the small increase in pH after exposure to ammonia mentioned above.

Changes in the structure and chemistry of the materials after exposure to ammonia are also observed on X-ray diffraction patterns and are presented in Fig. 8. As expected the spectra for MOF-5–ED and MOF-5–GO–ED do not change significantly compared to the ones for the initial samples. Only an increased splitting in the peak at 2Θ about ~9.60° is detected and it indicates a distortion in the cubic symmetry of MOF-5.[46]

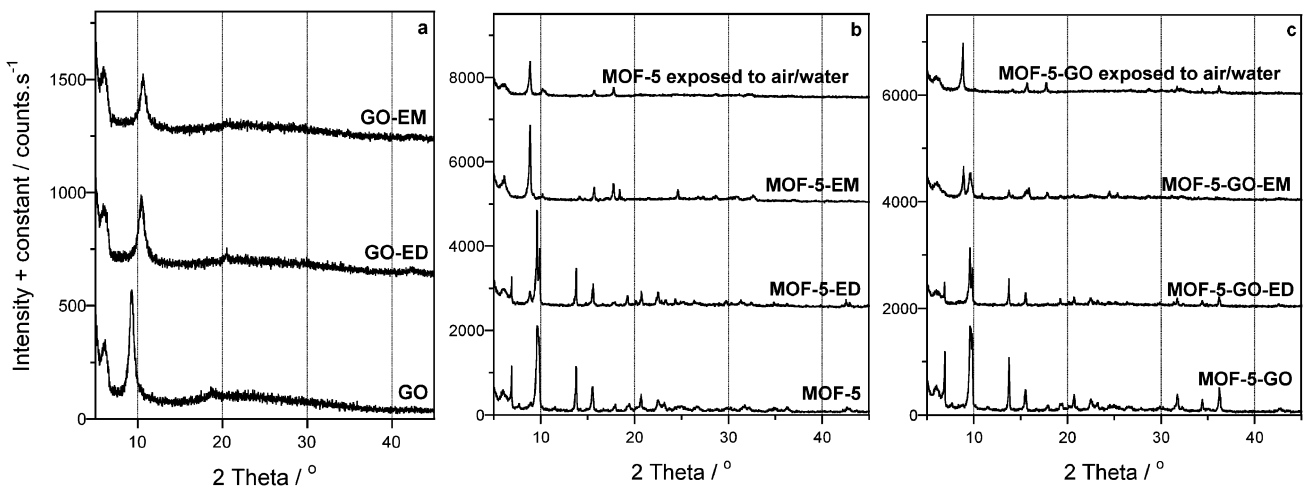

Fig. 8 X-Ray diffraction patterns for the initial and exhausted samples: (a) GO, (b) MOF-5, (c) MOF-5–GO.

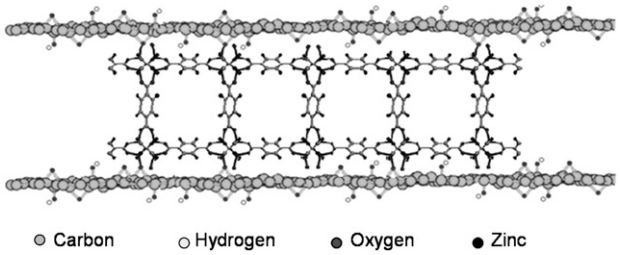

Fig. 9 A schematic view of the ideal composite structure; in light grey: carbon atoms; in white: hydrogen atoms, in dark grey: oxygen atoms, in black: zinc atoms.

The MOF-5–EM spectrum is similar to the one for MOF-5 exposed to humid air only and indicates once again the collapsing of the MOF-5 structure. For MOF-5–GO–EM, however, the spectrum is different from the one observed when the composite is exposed to moist air only. Two peaks at 2Θ about 9.65° and 8.90° are detected. A possible explanation would be that the first peak (9.65°) belongs to the initial MOF-5 structure while the second one (8.90°) comes from the decomposed compound. This supports the hypothesis about the differences in the mechanism of destruction when ammonia together with water is present in the challenge gas and suggests different stability of MOF-5 when combined with graphite oxide.

As described above, water has a contradictory effect on ammonia adsorption on the MOF-5 and MOF-5–GO samples. On the one hand, it decomposes the MOF-5 structure and releases carboxylic groups able to interact with ammonia and thus enhances ammonia adsorption. On the other hand, it leads to the decomposition of the material and thus to the destruction of the pore space where ammonia can be stored. Considering all these, ways to enhance ammonia adsorption without destroying the composite structure should be envisioned. Among the possible paths, one would be to have a composite with a regular alternation of one layer of GO and one layer of MOF-5 crystallites as opposed to the alternation of several stacked graphene layers with layers of MOF-5 blocks. In this case, the dispersive forces would be even more increased. A schematic view of this ideal composite is presented in Fig. 9. Another possible way to increase the performance of the composite might be to increase the chemical heterogeneity of the surface using a MOF compound with functionalities on the benzene rings able to interact with ammonia (without interfering with the composite formation).

Conclusion

The results presented in this paper describe the synthesis and properties of a new material, MOF-5–GO nanocomposite. The material obtained has a unique layered texture with a preserved structure of MOF-5 and GO. When tested as an ammonia adsorbent, the composite shows some synergy enhancing the adsorption capacity in comparison with the hypothetical physical mixture of components. Although the removal capacity is high in the presence of moisture, water has a detrimental effect on the chemistry of MOF-5 based materials and destroys the porous frameworks. Carboxylic groups from the MOF-5 structure are released during the material's collapse and are then able to interact with ammonia. These processes (collapse of the structure and ammonia interaction with MOF-5 carboxylic groups) can also occur simultaneously owing to the competition between water and ammonia for the most reactive centers. This destruction of MOF-5 within the composite structure causes slow desorption of ammonia when the samples are purged with air due to the progressive removal of water in which it is dissolved.

Acknowledgements

This work was supported by the ARO (Army research office) grant W911NF-05-1-0537 and the NSF Collaborative grant 0754945/0754979.

References

1 B. C. Brodie, *Ann. Chim. Phys.*, 1860, **59**, 466.
2 A. Buchsteiner, A. Lerf and J. Pieper, *J. Phys. Chem. B*, 2006, **110**, 22328.
3 T. Szabó, O. Berkesi and I. Dékány, *Carbon*, 2005, **43**, 3186.
4 A. Lerf, H. He, M. Forster and J. Klinowski, *J. Phys. Chem. B*, 1998, **102**, 4477.
5 T. Szabó, O. Berkesi, P. Forgó, K. Josepovits, Y. Sanakis, D. Petridis and I. Dékány, *Chem. Mater.*, 2006, **18**, 2740.
6 M. Seredych and T. J. Bandosz, *Carbon*, 2007, **45**, 2130.
7 M. Seredych and T. J. Bandosz, *J. Phys. Chem. C*, 2007, **111**, 15596.
8 Z.-H. Liu, Z.-M. Wang, X. Yang and K. Ooi, *Langmuir*, 2002, **18**, 4926.
9 A. B. Bourlinos, D. Gournis, D. Petridis, T. Szabo, A. Szeri and I. Dekany, *Langmuir*, 2003, **19**, 6050.
10 C. Nethravathi and M. Rajamathi, *Carbon*, 2006, **44**, 2635.
11 Y. Matsuo, K. Hatase and Y. Sugie, *Chem. Mater.*, 1998, **10**, 2266.
12 Y. Matsuo, Y. Matsumoto, T. Fukutsuka and Y. Sugie, *Carbon*, 2006, **44**, 3134.
13 X. Yang, Y. Makita, Z.-H. Liu and K. Ooi, *Chem. Mater.*, 2003, **15**, 1228.
14 J. Li, L. Vaisman, G. Marom and J.-K. Kim, *Carbon*, 2007, **45**, 744.
15 K. Morishige and T. Hamada, *Langmuir*, 2005, **21**, 6277.
16 Z. Mo, Y. Sun, H. Chen, P. Zhang, D. Zuo, Y. Liu and H. Li, *Polymer*, 2005, **46**, 12670.
17 Y. H. Chu, Z.-M. Wang, M. Yamagishi, H. Kanoh, T. Hirotsu and Y.-X. Zhang, *Langmuir*, 2005, **21**, 2545.
18 Z.-M. Wang, K. Shishibori, K. Hoshinoo, H. Kanoh and T. Hirotsu, *Carbon*, 2006, **44**, 2479.
19 M. Seredych, A. V. Tamashausky and T. J. Bandosz, *Carbon*, 2008, **46**, 1241.
20 T. Szabó, E. Tombácz, E. Illés and I. Dékány, *Carbon*, 2006, **44**, 537.
21 M. Hirata, T. Gotou, S. Horiuchi, S. Fujiwara and M. Ohba, *Carbon*, 2004, **42**, 2929.
22 M. Seredych, C. Petit, A. V. Tamashausky and T. J. Bandosz, *Carbon*, 2009, **47**, 445.
23 C. Petit, C. Karwacki, G. Peterson and T. J. Bandosz, *J. Phys. Chem. C*, 2007, **111**, 12705.
24 O. M. Yaghi and H. Li, *J. Am. Chem. Soc.*, 1995, **117**, 10401.
25 O. M. Yaghi, H. Li and T. L. Groy, *J. Am. Chem. Soc.*, 1996, **118**, 9096.
26 M. Eddaoudi, H. Li and O. M. Yaghi, *J. Am. Chem. Soc.*, 2000, **122**, 1391.
27 J. Kim, B. Chen, T. M. Reineke, H. Li, M. Eddaoudi, D. M. Moler, M. O'Keeffe and O. M. Yaghi, *J. Am. Chem. Soc.*, 2001, **123**, 8239.
28 W.-G. Lu, C.-Y. Su, T.-B. Lu, L. Jiang and J. M. Chen, *J. Am. Chem. Soc.*, 2006, **128**, 34.
29 N. W. Ockwig, O. Delgado-Friedrichs, M. O'Keeffe and O. M. Yaghi, *Acc. Chem. Res.*, 2005, **38**, 176.
30 J. Hafizovic, A. Krivokapic, K. C. Szeto, S. Jakobsen, K. P. Lillerud, U. Olsbye and M. Tilset, *Cryst. Growth Des.*, 2007, **7**, 2302.
31 Z. Wang and S. M. Coehn, *J. Am. Chem. Soc.*, 2007, **129**, 12368.
32 A. P. Cote, H. M. El-Kaderi, H. Furukawa, J. R. Hunt and O. M. Yaghi, *J. Am. Chem. Soc.*, 2007, **129**, 12914.

33 S. L. Gould, D. Tranchemontagne, O. M. Yaghi and M. A. Garcia-Garibay, *J. Am. Chem. Soc.*, 2008, **130**, 3246.
34 K. S. Walton and R. Q. Snurr, *J. Am. Chem. Soc.*, 2007, **129**, 8552.
35 M. Eddaoudi, J. Kim, N. Rosi, D. Vodak, J. Wachter, M. O'Keeffe and O. M. Yaghi, *Science*, 2002, **295**, 469.
36 D. Britt, D. Tranchemontagne and O. M. Yaghi, *Proc. Natl. Acad. Sci. U. S. A.*, 2008, **105**, 11623.
37 Q. Yang and C. Zhong, *J. Phys. Chem. B*, 2006, **110**, 655.
38 U. Mueller, M. Schubert, F. Teich, H. Puetter, K. Schierle-Arndt and J. Pastre, *J. Mater. Chem.*, 2006, **16**, 626.
39 B. Chen, S. Ma, E. J. Hurtado, E. B. Lobkovsky, C. Liang, H. Zhu and S. Dai, *Inorg. Chem.*, 2007, **46**, 8705.
40 A. R. Millward and O. M. Yaghi, *J. Am. Chem. Soc.*, 2005, **127**, 17998.
41 D. Y. Siberio-Perez, A. G. Wong-Foy, O. M. Yaghi and A. J. Matzger, *Chem. Mater.*, 2007, **19**, 3681.
42 H. Li, M. Eddaoudi, M. O'Keeffe and O. M. Yaghi, *Nature*, 1999, **402**, 276.
43 W. S. Hummers and R. E. Offeman, *J. Am. Chem. Soc.*, 1958, **80**, 1339.
44 C. M. Lastoskie, K. E. Gubbins and N. Quirke, *J. Phys. Chem.*, 1993, **97**, 4786.
45 S. S. Kaye, A. Dailly, O. M. Yaghi and J. R. Long, *J. Am. Chem. Soc.*, 2007, **129**, 14176.
46 J. Hafizovic, M. Bjørgen, U. Olsbye, P. D. C. Dietzel, S. Bordiga, C. Prestipino, C. Lamberti and K. P. Lillerud, *J. Am. Chem. Soc.*, 2007, **129**, 3612.
47 L. Huang, H. Wang, J. Chen, Z. Wang, J. Sun, D. Zhao and Y. Yan, *Microporous Mesoporous Mater.*, 2008, **58**, 105.
48 J. A. Greathouse and M. D. Allendorf, *J. Am. Chem. Soc.*, 2006, **120**, 10678.
49 C. Petit and T. J. Bandosz, *Adv. Funct. Mater.*, submitted.
50 B. Panella and M. Hirscher, *Adv. Mater.*, 2005, **17**, 538.
51 J. C. Thompson, *Phys. Rev. A*, 1971, **4**, 802.
52 K. Schröck, F. Schröder, M. Heyden, R. A. Fischer and M. Havenith, *Phys. Chem. Chem. Phys.*, 2008, **10**, 4732.
53 J. Helminen, J. Helenius and E. Paatero, *J. Chem. Eng. Data*, 2001, **46**, 391.
54 L. M. Le Leuch and T. J. Bandosz, *Carbon*, 2007, **45**, 568.
55 C. Petit and T. J. Bandosz, *J. Phys. Chem. C*, 2007, **111**, 16445.
56 C. Petit and T. J. Bandosz, *Microporous Mesoporous Mater.*, 2008, **114**, 137.
57 C. Petit and T. J. Bandosz, *Environ. Sci. Technol.*, 2008, **42**, 3033.
58 C. Petit and T. J. Bandosz, *Microporous Mesoporous Mater.*, 2009, **118**, 61.
59 C. Petit and T. J. Bandosz, *J. Colloid Interface Sci.*, 2008, **325**, 301.
60 C. L. McCallum, T. J. Bandosz, S. C. McGrother, E. A. Müller and K. E. Gubbins, *Langmuir*, 1999, **15**, 533.
61 T. Szabó, O. Berkesi and I. Dékány, *Carbon*, 2005, **43**, 3186.
62 N. I. Kovtyukhova, P. J. Ollivier, B. R. Martin, T. E. Mallouk, S. A. Chizhik, E. V. Buzaneva and A. D. Gorchinskiy, *Chem. Mater.*, 1999, **11**, 771.
63 S. Hermes, F. Schröder, S. Amirjalayer, R. Schmid and R. A. Fischer, *J. Mater. Chem.*, 2006, **16**, 2464.
64 E. Biemmi, T. Bein and N. Stock, *Solid State Sci.*, 2006, **8**, 363.
65 J. Zawadzki and M. Wisniewski, *Carbon*, 2003, **41**, 2257.
66 Y. Wang, B. Bredenkotter, B. Riegera and D. Volkmer, *Dalton Trans.*, 2007, 689.

